Int. J. Electrochem. Sci., 12 **(2017)** 7227 – 7239, doi: 10.20964/2017.08.01

International Journal of
ELECTROCHEMICAL
SCIENCE
www.electrochemsci.org

One-step Preparation of Alkaline Lignin-based Activated Carbons with Different Activating Agents for Electric Double Layer Capacitor

*Yan Wu, Jing-Pei Cao**, *Zhi-Qiang Hao, Xiao-Yan Zhao***, *Qi-Qi Zhuang, Jun-Sheng Zhu, Xing-Yong Wang, Xian-Yong Wei*

Key Laboratory of Coal Processing and Efficient Utilization (Ministry of Education), China University of Mining & Technology, Xuzhou 221116, Jiangsu, China
*E-mail: caojingpei@cumt.edu.cn; beyondcao@hotmail.com; beyondcao_2000@163.com
**E-mail: zhaoxiaoyan@cumt.edu.cn

Received: 3 May 2017 / *Accepted:* 29 May 2017 / *Published:* 12 July 2017

Different structured activated carbons (ACs) were made from lignin (alkaline) by one-step activation. Using $ZnCl_2$, KOH and K_2CO_3 as activating agents and the effect of activating agents on the electrochemical properties of the ACs for electric double layer capacitor (EDLC). The ACs prepared by the three kinds of activating agents are mainly microporous, while the $ZnCl_2$-activated and KOH-activated ACs contain mesoporous through the nitrogen adsorption-desorption test. All the ACs used as electrode for EDLC showed excellent cyclability. The small amount of CO_2 produced by K_2CO_3 decomposition involved in the activation reaction and a series of reactions between carbon of lignin and K_2CO_3, giving a AC with the maximum specific surface area of 1585 m^2 g^{-1}, and the best specific capacitance (C_s) performance of 263.46 F g^{-1} at the current density 40 mA g^{-1}, using a two-electrode system. The results indicate that the K_2CO_3 as activating agent to prepared lignin-based AC applied in EDLC is appropriate.

Keywords: Activated carbon; Activating agent; Lignin; EDLC; Specific capacitance.

1. INTRODUCTION

Supercapacitors is a kind of energy storage device between the tradition capacitor and secondary batteries, which has drawing much attention due to its high energy density, long cycle life and excellent reversibility [1, 2]. According to the mechanism of energy storage, the supercapacitors can be divided into electric double layer capacitor (EDLC, storing the charge electrostatically by using reversible adsorption of ions of the electrolyte), pseudo-capacitive (reversible redox reaction occurs on the surface of electrode materials) and hybrid capacitors (the combination of EDLC and constraint capacitance) [3, 4].

In present, the materials for EDLC electrode include activated carbons (ACs), carbon nanotubes, carbon aerogels, graphene sheets and carbon nanofibers [5-7]. Especially, the ACs with high specific surface area (SSA) have captured much interest attribute to its inexpensive price, rich raw material, good chemical stability and high electrical conductivity. Generally, the preparation methods of ACs include physical activation and chemical activation [8]. Physical activation consists of two steps, i.e., carbonization under inert atmosphere and activation through CO_2 or steam. While the chemical activated process is that the raw material is mixed with activating agent and heated in an inert atmosphere. Compared with physical activation, chemical activation has two significant advantages. One is that the temperature of the chemical activation is low. The other is that the global yield of the chemical activation trends to be greater since burn-off char is not required [9].

Nowadays, the method of preparing ACs is mainly chemical activation because the ACs prepared by chemical activation have present higher SSA, lower activation time, higher yield and better pore structure in comparison to physical activation [10]. It is well known that the ideal ACs for EDLC electrodes should have high SSA and appropriate pore size distribution (PSD), which are important parameters for high specific capacitance (C_s) of EDLC [11, 12]. Therefore, it is important to choose the activating agent and match the precursor. The ACs prepared with different activating agents possess different properties, such as SSA, PSD and morphology. The electrochemical properties of EDLC are significantly impacted by the propertied of ACs.

Lignin is the second most abundant natural organic matter next to cellulose in the world. Low cost and abundance of hydroxyl group make lignin becomes preferred precursor for preparation of ACs. KOH and $ZnCl_2$ as activating agents were widely used in various precursors [13-16]. It is known that KOH is a strong base, $ZnCl_2$ is a Lewis acid and K_2CO_3 is a weak base. They have different chemical nature and activation mechanism in the activation process, which leading to the property of ACs are different. Xiang et al. [17] prepared ACs from polyaniline by K_2CO_3 activation and found that the SSA of AC with K_2CO_3 is much larger than that without K_2CO_3. However, there are few studies on the preparation of ACs used the same precursor with different activating agents for EDLC.

In this work, ACs were prepared from lignin by chemical activation with different activating agents including KOH, K_2CO_3 and $ZnCl_2$. The ACs were characterized by nitrogen adsorption-desorption isotherms, scanning electron microscope (SEM), Fourier transform infrared spectroscopy (FTIR) and Raman. The ACs were used as electrode for EDLC and the electrochemical properties were studied by cyclic voltammetry (CV) and galvanostatic charge-discharge (GCD).

2. EXPERIMENTAL

2.1. Materials and Reagents

Lignin (alkaline) purchased from TCI was employed to prepared ACs. Table 1 shows its proximate and ultimate analyses of the lignin. $ZnCl_2$, KOH and K_2CO_3 are provided by Xilong Chemical Co. Ltd. Deionized water was used through all the experiment.

Table 1. Proximate and ultimate analyses of lignin.

Sample	Proximate analysis (wt%)				Ultimate analysis (wt%, daf)				
	M_{ar}	A_d	VM_d	FC_d^a	C	H	N	S	O^a
Lignin	4.03	16.76	48.66	34.57	64.91	7.34	0.26	7.67	19.82

A: ash; M: moisture; VM: volatile matter; FC: fixed carbon; ar: as received basis; d: dried basis; a: by difference.

2.2. Preparation of Lignin-based AC

One-step preparation of alkaline lignin-based ACs were performed using lignin impregnating with different activating agents with a weight ratio of 1:1. Then the mixture was heat up to 700 ^oC for 60 min under nitrogen atmosphere in a horizontal tube furnace. After being cooled, the activated samples were washed with 2 M HCl, filtered and rinsed by warm distilled water several times, and then washed by room-temperature distilled water until the filtrate became neutral. The washed sample was dried in vacuum oven at 150 ^oC for 3 h. The samples were denoted as LAC, LAC-Z, LAC-K and LAC-K_2 which represents without activating reagent, activated by $ZnCl_2$, KOH and K_2CO_3, respectively. The yield of the ACs was calculated by following formula:

$$Y = \frac{M_1}{M_2} \times 100\% \qquad (1)$$

Where M_1 is the weight of ACs and M_2 is the weight of lignin.

2.3. Characterization

Thermogravimetric (TG) analysis of lignin was taken on a Mettler Toledo TGA/DSC1 to investigate the thermal behavior of lignin. A Nicolet Magna 560 FTIR and a Merlin Zeiss SEM were used to observe the surface functional groups and the surface morphology of the obtained samples. Raman scattering spectra were recorded using a Bruker Senterra dispersive Raman spectrometer with 532 nm laser excitation. Nitrogen adsorption-desorption isotherms were carried out at 77 K on a Gold APP V-Sorb 4800TP surface area and pore size analyzer. Brunauer-Emmett-Teller (BET) formula and Density Functional Theory (DFT) were used to calculate the SSA and PSD. The total pore volume (V_t) was determined at a relative pressure of $P/P_0 = 0.99$. The micropore surface area (S_{mic}) and micropore volumes (V_{mic}) were performed on the t-plot method. The external area (S_{ext}) and the external volume (V_{ext}) were obtained by the difference of S_{mic} from SSA and difference of V_{mic} from V_t.

2.4. Electrochemical Measurements

The electrodes of EDLC were prepared by mixing 85wt.% AC, 10wt.% acetylene black and 5wt.% polytetrafluoroethylene (PTFE) binder in an agate mortar and then pressed onto Ni foil, which was used as the current collector. The diameter of electrode was 13 mm. The electrochemical measurement was tested using MTI EQ-STC two-electrode system with 6 M KOH solution as electrolyte. The polypropylene membrane was used as the separator. CV was carried out at different scan rates with a voltage ranging from 0 to 1 V. Electrochemical impedance spectroscopy (EIS) measurements were measured at the open circuit voltage with amplitude of 10 mV and the frequency range from 10^{-2} to 10^{5} Hz. CV and EIS were tested on an Ivium Vertex electrochemical workstation. The GCD test was performed in a potential range of 0.0-0.9 V on a NEWARE cell test instrument. The C_s was calculated by following equation according to discharge curve.

$$C_s = 2\frac{I\Delta t}{m\Delta V} \qquad (2)$$

Where I is the current of discharge, Δt is the discharge time and m is one of the mass of electrodes material, ΔV is the voltage difference.

3. RESULTS AND DISCUSSION

3.1. TG Analysis of Lignin

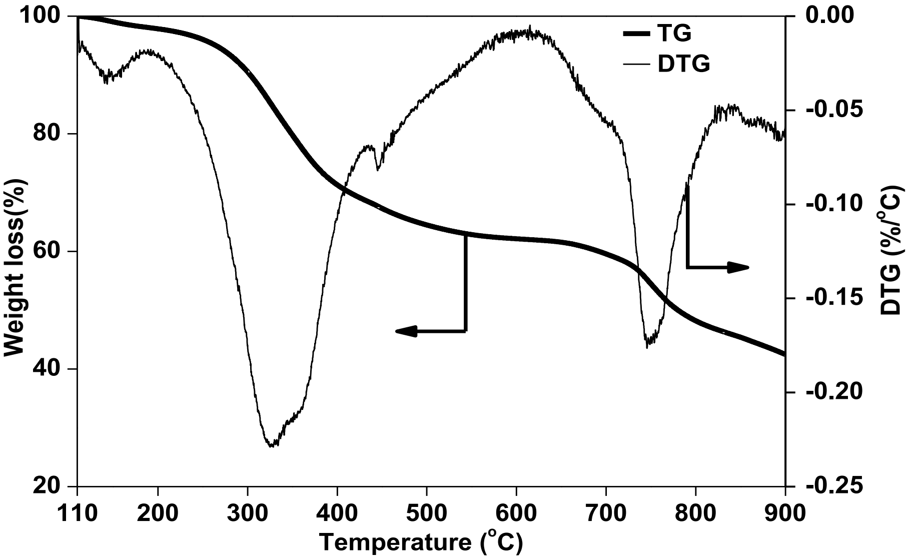

Figure 1. TG and DTG curves of lignin.

TG and derivative thermogravimetry (DTG) curves of lignin are depicted in Fig. 1. It can be easily seen that the weight loss of lignin is divided into three steps. The weight loss below 200 °C is attributed to the elimination of moisture and some volatile substances. The second stage from 200 °C to 500 °C should be due to the decomposition of oxygen-containing functional groups linked to carbon in lignin. The release of CO_2 and CO is at this stage [18, 19]. The third weight loss ranging from 500 °C to 800 °C is about 13.99%, which is attributed to the undecomposed and unstable carbon. Lignin pyrolysis takes place at a relatively wide temperature ranging from 200 to 800 °C, indicating a stable characteristic [18, 20].

3.2. Structure Characterization of Lignin-based ACs

3.2.1. Nitrogen Adsorption-desorption Isotherms

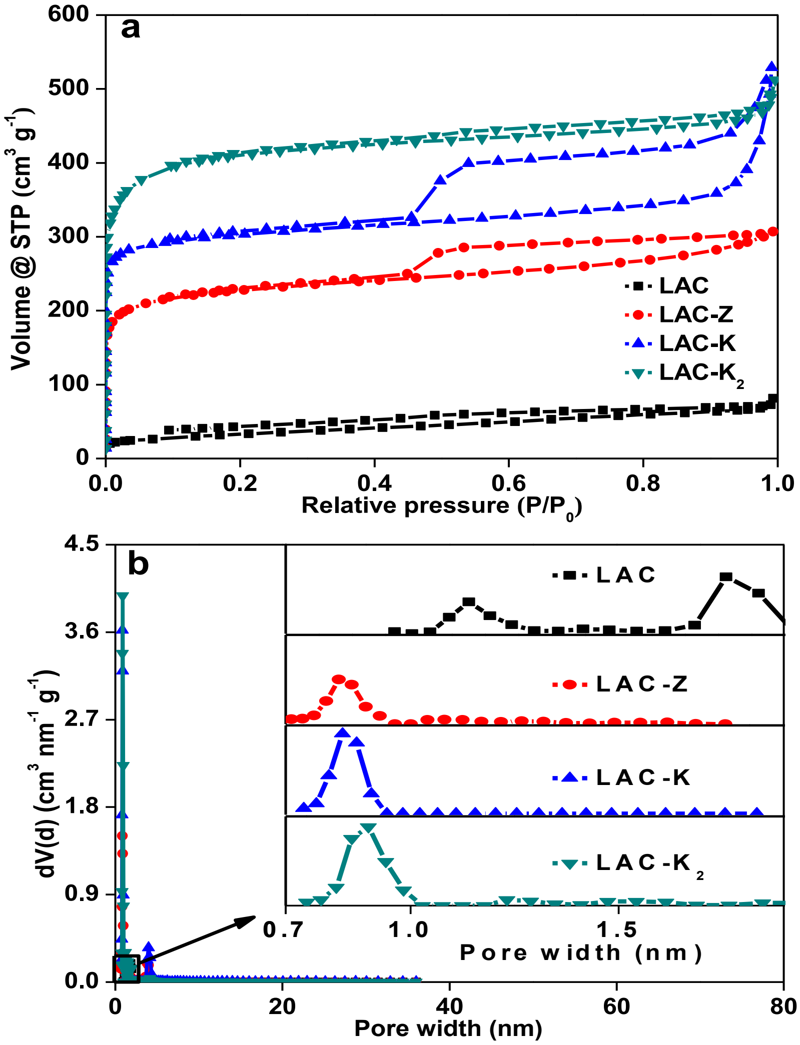

Figure 2. (a) Nitrogen adsorption-desorption isotherms; (b) PSD of ACs.

Fig. 2 shows the nitrogen adsorption-desorption isotherms and PSD of ACs made by different activating agents. The porous structure parameters are summarized in Table 2. As shown in Fig. 2a, all the nitrogen adsorption-desorption isotherms of samples are belong to type I according to the IUPAC classification [21]. LAC has lower adsorption capacities than LAC-Z, LAC-K and LAC-K_2, especially at low pressure, indicating the presence of less micropores. The adsorption capacities increased significantly after activation, illustrating a large number of micropores existed in the LAC-Z, LAC-K and LAC-K_2. A high uptake was observed in relatively low pressure region demonstrates the existence of abundant micropores [18]. There are obvious hysteresis loop and a slightly tail in all the samples at high P/P_0 value, which demonstrate the presence of mesopores and macropores, especially for LAC-Z, LAC-K and LAC-K_2. Meanwhile, the AC activated with K_2CO_3 has larger adsorption volume than by $ZnCl_2$ and KOH, which shows the AC activated by K_2CO_3 has a higher SSA than $ZnCl_2$-activated and

KOH-activated. The SSA of LAC, LAC-Z, LAC-K and LAC-K_2 is 116, 866, 1191 and 1585 m^2 g^{-1}, respectively (Table 2).

As can be deduced from Fig. 2b, the pore diameters of all the samples are less than 5 nm, indicating that the AC is mainly micropore and mesopore. The pore size of LAC mainly distribute in 1.18 nm and 1.88 nm. There are some pores in size of 2.43 nm to 4.16 nm of LAC. The pore size of LAC-Z, LAC-K and LAC-K_2 is mainly in 0.86, 0.87 and 0.91 nm, respectively. In addition, a part of the pore sizes of LAC-Z and LAC-K is in the range of 3.63-4.32 and 3.64-4.37 nm. The results are well consistent with the curves of nitrogen adsorption-desorption, in which that the AC by K_2CO_3 activation is mainly micropores.

Table 2. Porous structure parameters of lignin-based ACs prepared at various activating reagents.

Sample	S_{BET} (m^2 g^{-1})	V_{tot} (m^3 g^{-1})	S_{mic} (m^2 g^{-1})	S_{ext} (m^2 g^{-1})	V_{mic} (cm^3 g^{-1})	V_{ext} (cm^3 g^{-1})	D_e (nm)	Yield (%)
LAC	116	0.13	28	88	0.013	0.117	4.31	47.73
LAC-Z	866	0.47	741	125	0.30	0.17	2.19	48.06
LAC-K	1191	0.82	1065	126	0.42	0.40	2.75	34.61
LAC-K_2	1585	0.79	1479	106	0.59	0.20	1.99	19.75

S_{BET}: BET surface area; V_{tot}: total pore volume; S_{mic}: micropore surface area; S_{ext}: external surface area; V_{mic}: micropore volume; V_{ext}: external volume; D_e: average pore diameter. External surface area was calculated by S_{BET}-S_{mic} and external volume was calculated by V_{tot}-V_{mic}.

It can be seen from Table 2 that the LAC-K_2 has the highest SSA and LAC-K has the highest V_{tot} and V_{ext} among all the samples. The SSA of LAC-Z is the minimum and the V_{tot} of LAC-Z is between the LAC-K and LAC-K_2, which suggests that the activation mechanisms of $ZnCl_2$ is different from alkali metal compounds. The activated mechanisms will be discussed below. The SSA of the ACs activated by activating agents is much larger than that without activating agent (LAC), indicating addition of activator is beneficial for the preparation of ACs with large SSA. The $ZnCl_2$ acts as dehydration reagent and it restricts the formation of tar and promotes the aromatization [22], which leads to the maximum yield of AC.

3.2.2. SEM Analysis

SEM images of the prepared lignin-based ACs are shown in Fig. 3. It can be seen that obvious cavities exist in the external surface of the ACs. Moreover, the ACs activated by $ZnCl_2$, KOH and K_2CO_3 have more abundant pore structure. The cavities on the surface of LAC-Z resulted from $ZnCl_2$ evaporation during the activated process, leaving the position previously occupied by the $ZnCl_2$ [14]. There are a lot of micropores on the LAC-K (Fig. 3c), demonstrating that the gasification of carbon occurs on the external surface during the carbonization process [23]. Fig. 3d shows the LAC-K_2 contains many particles and the surface is unevenness and disorder. The particles are small and contact more closely. The difference of surface morphology of ACs should be lead to the difference in electrochemical performances.

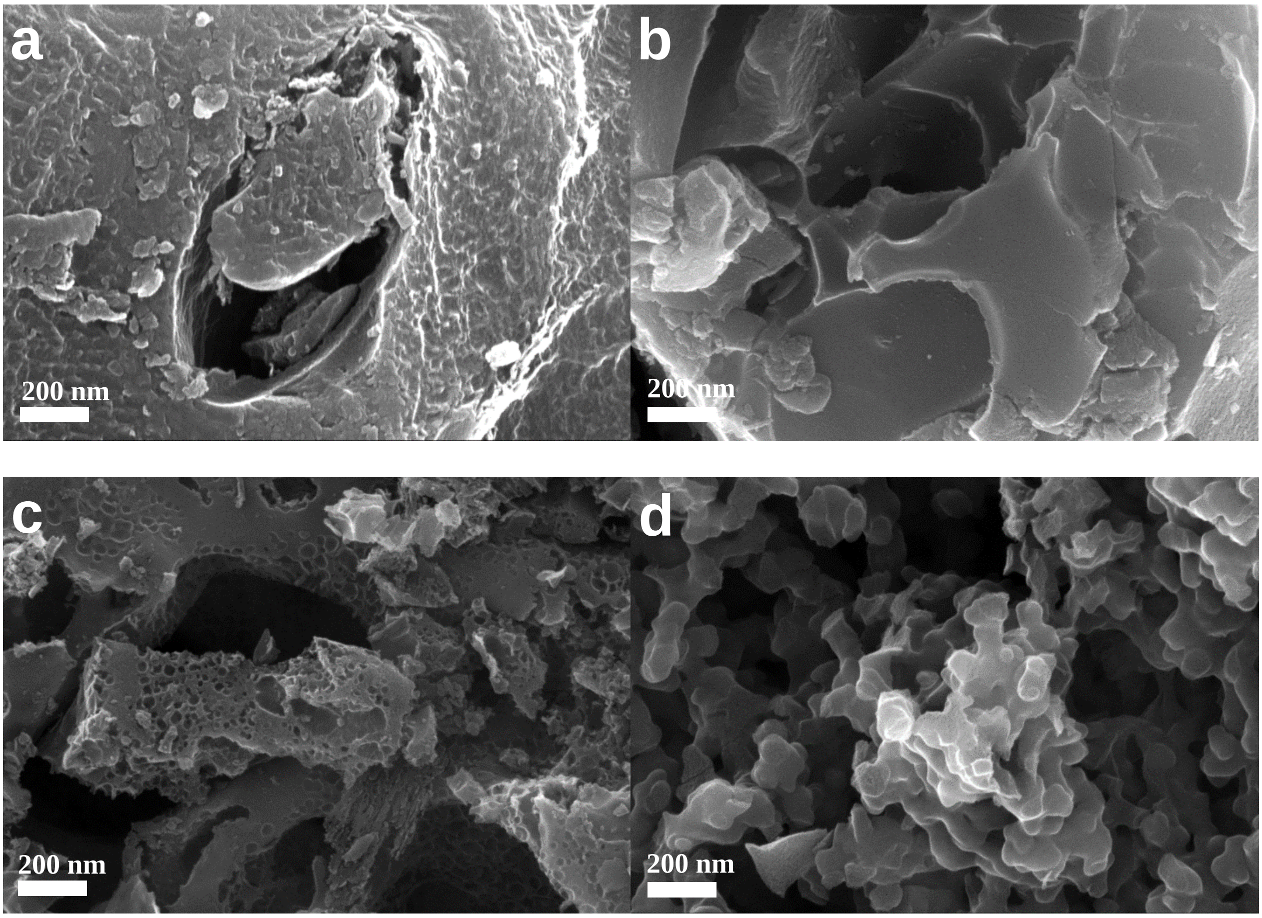

Figure 3. SEM images of ACs: (a) LAC; (b) LAC-Z; (c) LAC-K; (d) LAC-K_2.

3.2.3. FTIR and Raman Analysis

FTIR spectroscopy was used to identify the functional groups of substances [24]. As shown in Fig. 4a, all the samples exhibit similar FTIR spectra, indicating the functional group of AC remains almost intact after activation. The strong band at 3421 cm^{-1} ascribing to -OH stretching vibration. Another strong band at 1622 cm^{-1} represents the aromatic skeletal vibrations. The weak bands at 1399 and 980 cm^{-1} indicative of C-H and C-O-C vibrations, respectively [25, 26]. The presence of peaks at 607 cm^{-1} is C-C out of plane bending [18]. The existence of oxygen-containing functional groups can improve the wettability of the AC surface, which is beneficial to enhance the electrochemical performance [27, 28]. The Raman scattering spectra of the ACs are given in Fig. 4. The strong band at approximately 1342 cm^{-1} (D-band) is associated to the disordered amorphous carbon (tetrahedral sp^3 coordination) and the peak at around 1587 cm^{-1} (G-band) is attributed to the ordered graphitic carbon (planar sp^2 coordination) [29]. In general, the relative intensity of D/G stand for the degree of graphite. The I_D/I_G ratio of LAC, LAC-Z, LAC-K and LAC-K_2 is 0.87, 0.79, 0.88 and 0.93, respectively.

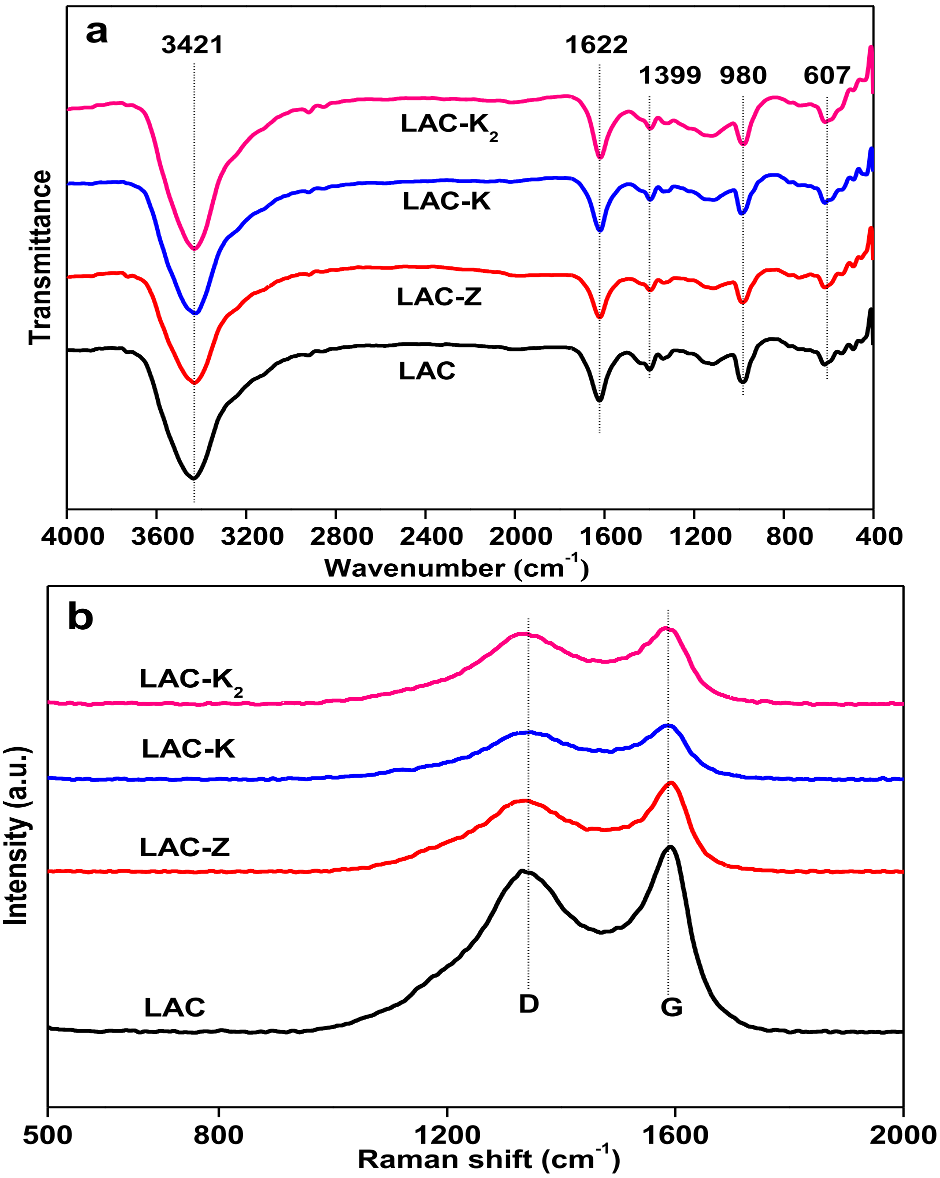

Figure 4. (a) FTIR and (b) Raman spectra of ACs.

The ACs activated by KOH and K_2CO_3 show more defects and disordered graphite, which may be due to the intercalation of potassium into AC at 700 °C, leading to the disorder degree of AC. The result coincides with the SEM, which can be found from Figs. 3c and 3d that the surface of LAC-K and LAC-K_2 are uneven. Hayashi et al. [30] reported that the optimal activated temperature of lignin by $ZnCl_2$ is 600 °C. In this work, the temperature of 700 °C may leads to heat shrinkage and thus results in the increase in graphitization degree. Therefore, the I_D/I_G of LAC-Z is smaller than other ACs.

3.3. Electrochemical of the ACs

Fig. 5a shows the GCD curves of ACs at the current density of 40 mA g^{-1} in the potential range of 0-0.9 V. All the curves of charge-discharge exhibited high symmetry and linearity with low iR drops, indicating good EDLC behaviors [31, 32]. The charge-discharge times of LAC-Z, LAC-K and LAC-K_2 are much longer than LAC, indicating the C_s of LAC-Z, LAC-K and LAC-K_2 is higher than LAC at the same current density and also suggesting that the electrochemical performance are improved significantly with the activating agents treated. The C_s can be calculated according to the formula (2) and the results are listed in Table 3. The charge-discharge time of LAC-K and LAC-K_2 are nearly equal, indicating the C_s of LAC-K and LAC-K_2 are approach. This is because of the presence of large amount of mesoporous in LAC-K and the highest SSA of LAC-K_2. Several studies [33-36] reported that the C_s is affected not only by the SSA but also by the pore size. The higher SSA of ACs, the more energy interface can storage. The appropriate pore size is favorable for the transmission of ions and the obtaining a large C_s [37].

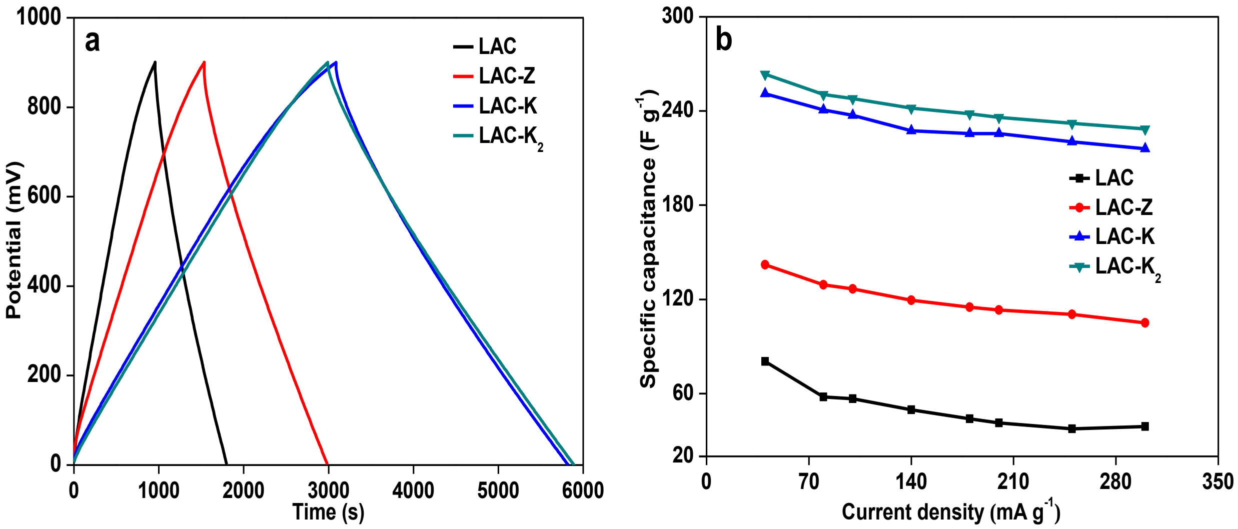

Figure 5. (a) GCD curves of ACs at 40 mA g^{-1} and (b) the specific capacitance of ACs at different current densities.

Table 3. The electrochemical performance of different samples in two-electrode system.

Sample	Capacitance (F g^{-1}) 40 (mA g^{-1})	80 (mA g^{-1})	100 (mA g^{-1})	140 (mA g^{-1})	180 (mA g^{-1})	200 (mA g^{-1})	250 (mA g^{-1})	300 (mA g^{-1})
LAC	69.83	57.82	57.70	49.61	43.99	41.22	39.07	37.54
LAC-Z	142.09	129.22	126.68	119.41	114.95	113.18	110.38	104.98
LAC-K	251.04	240.72	237.19	227.46	225.57	221.87	220.36	215.91
LAC-K_2	263.46	250.60	247.85	241.88	238.21	236.02	232.21	228.56

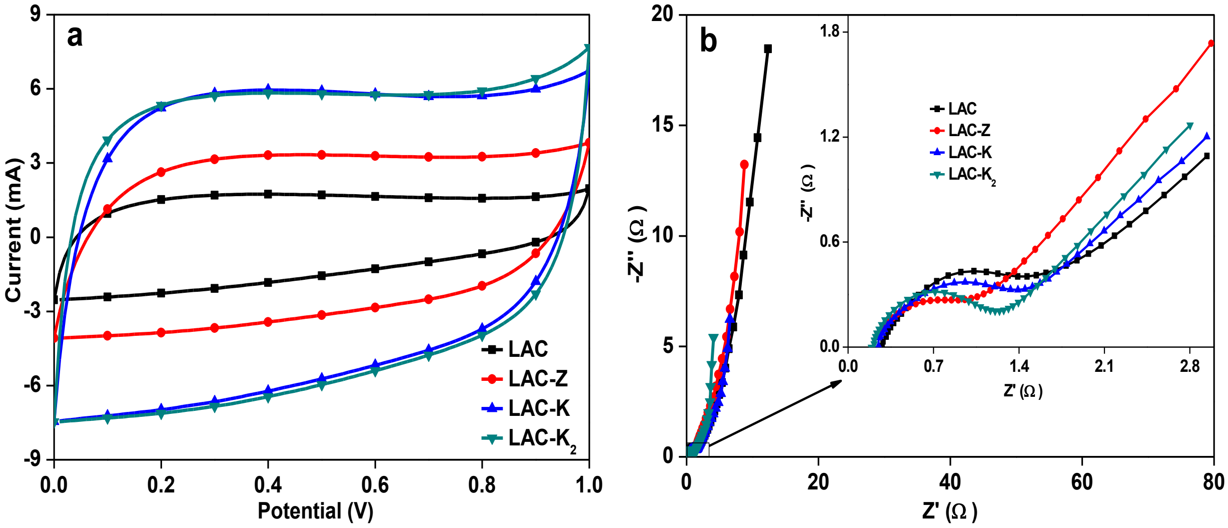

Figure 6. (a) CV curves for ACs at scan rate of 2 mV s^{-1} and (b) Nyquist plots of the ACs electrodes and the inset is the enlarged plots of the high-frequency region.

Fig. 5b shows the relationship between the C_s and current density. Table 3 summarizes the C_s of all the samples under different current densities calculated from the GCD curves. The C_s of all the samples dropped with increasing current density. And the decrease amplitude of LAC-Z, LAC-K and LAC-K_2 is smaller than KAC in Fig. 5b, which due to the difference of SSA and PSD. At low current density, the electrolyte ions have enough time into the micropores and the available surface of micropores is reduced at high current density. It is well known that the diffusion of electrolyte ions into the micropores suffers great resistance and the electrolyte ions have difficulty in entering the micropores in a short time at high current density [32, 38].

Fig. 6a illustrates the CV curves of all the samples at scan rate of 2 mV s^{-1}. All the CV curves are approximately rectangular without obviously redox peaks, which indicated that the C_s mainly provide by EDLC [39]. The areas of the CV curves represents the value of C_s. In addition, the areas of LAC-K_2 and LAC-K are approximately equal, which indicating the C_s of the LAC-K_2 and LAC-K is close. Meanwhile, the CV curve areas of LAC-Z, LAC-K and LAC-K_2 are larger than the LAC, demonstrating that C_s of LAC is smaller than others. All the results can be also obtained from the GCD curves in Fig. 5a.

Fig. 6b shows the Nyquist plots of ACs electrodes in the frequency range of 10^{-2} to 10^{5} Hz under the open circuit potential. At low-frequency region, the lines is nearly vertical to the $Z^{'}$ axis, which indicating the ACs electrodes have good electrochemical capacitance behavior. All the plots of samples display a small semicircle at high-frequency. The semicircle represents the transfer resistance of the charge-discharge at the electrode/electrolyte interface [40]. The intercept of plot with the $Z^{'}$ axis is the equivalent series resistance (ESR, R_s), which includes the resistance of electrolyte, resistance of the material and the contact resistance of collector with materials [41]. The R_s of LAC-K_2 is 0.19 Ω, which is lower than of LAC-K (0.25 Ω) and LAC-Z (0.31 Ω). There is a line with the slop close to 45° in the middle frequency range, which is the Warburg impedance (W). The W represent the diffusion resistance of electrolyte [42]. As shown in the insert of Fig. 6b, the LAC-Z and LAC-K have short Warburg-type line, suggesting the micro-mesoporous structure is favorable for ion diffusion.

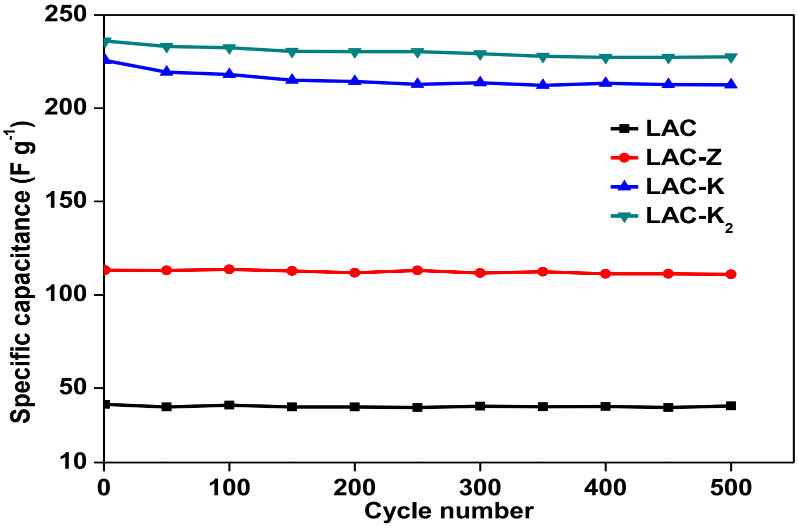

Figure 7. Cycle performance of ACs at 200 mA g^{-1} in 6 M KOH solution.

For better understanding the electrochemical stability of EDLC, cycle performance is measured and shown in Fig. 7. The retention rate of C_s after 500 cycles for LAC, LAC-Z, LAC-K and LAC-K$_2$ is about 97.74%, 97.99%, 95.82% and 96.41%, respectively, which demonstrating the superior cycling stability in the 6 M KOH electrolyte at a current density of 200 mA g^{-1}.

3.4. Activation Process

Lignin is a kind of high molecular polymer and three major structures of lignin, i.e, 4-hydroxyphenyl, guaiacyl, and syringyl structures [43] and lignin have high carbon content. The hydroxyl groups in lignin structure are mainly aliphatic hydroxyl group and phenolic hydroxyl group, which leading to a strong reaction of lignin. In the activation process, the hydrogen and oxygen in lignin are released in the form of water vapor which leading to the formation of pore structure. Because of $ZnCl_2$ has catalytic effect on dehydroxylation and dehydration. KOH and K_2CO_3 not only as dehydrating agent but also as oxidant [44, 45]. The SSA of lignin-based AC activated by $ZnCl_2$ is smaller than the ACs with KOH and K_2CO_3. Moreover, there exist physical process during the K_2CO_3 activation process. The CO_2 produced by decomposition of K_2CO_3 involved in the activation reaction and a series of reactions between carbon of lignin and K_2CO_3, which leading to the AC prepared by K_2CO_3 has the maximum SSA.

$$K_2CO_3 \rightarrow K_2O + CO_2\uparrow \qquad (3)$$

$$\text{Lignin} + K_2CO_3 \rightarrow 2K + 3CO\uparrow \qquad (4)$$

Meanwhile, $ZnCl_2$ as a kind of Lewis acid can promote the reaction of aromatic condensation and inhibit the production of tar which leading to increase the yield of AC. And $ZnCl_2$ is evaporation at high temperature, leading to the transform of $ZnCl_2$ into the interior of carbon. Porous carbon was formatted after the $ZnCl_2$ washed by acid and water [23, 30]. A series of simple chemical reaction may take place between the KOH or K_2CO_3 and lignin ((3) ~ (6)). During KOH/K_2CO_3 activated process, some surface metal complexes are produced which may further improve the reaction with the carbon of lignin and the release of gaseous products such as CO and H_2. Thereby, an abundant of pore were formed on the surface of ACs and giving an amorphous carbon, which can be confirmed by SEM and Raman analysis.

$$\text{Lignin} + \text{KOH} \rightarrow \text{lignin.}K_2O + \text{lignin.}K_2CO_3 + H_2\uparrow \qquad (5)$$

$$K_2O + \text{Lignin} \rightarrow 2K + CO\uparrow \qquad (6)$$

4. CONCLUSION

ACs were obtained from lignin treated with $ZnCl_2$, KOH and K_2CO_3 by one-step carbonization and activation process. The functional groups of all the ACs are similar by the tested of FTIR, which showed that the activating agents had little effect on the functional groups of ACs. But the activating agents have great influence on the structure of ACs and all the ACs have higher SSA than that without activating agent. The SSA of LAC, LAC-Z, LAC-K and LAC-K_2 is 116, 866, 1191 and 1585 $m^2\ g^{-1}$, respectively, giving C_s of 69.83, 142.09, 251.04 and 263.46 F g^{-1} at a current density of 40 mA g^{-1} with 6 M KOH as the electrolyte. After 500 cycles, the EDLC show a stable performance, which the C_s retention of LAC, LAC-Z, LAC-K and LAC-K_2 is 97.74%, 97.99%, 95.82% and 96.41%, respectively.

ACKNOWLEDGEMENTS
This work was subsidized by the Fundamental Research Funds for the Central Universities (China University of Mining & Technology, Grant 2015QNA23), National Natural Science Foundation of China (Grant 21676292), Natural Science Foundation of Jiangsu Province (BK20161180), and the Priority Academic Program Development of Jiangsu Higher Education Institutions.

References

1. X. Zhang, L. Y. Ji, S. C. Zhang, W. S. Yang, *J. Power Sources*, 173 (2007) 1017.
2. Z. Q. Hao, J. P. Cao, Y. Wu, X. Y. Zhao, L. Zhou, X. Fan, Y. P. Zhao, X. Y. Wei, *Fuel Process. Technol.*, 162 (2017) 45.
3. T. A. Centeno, F. Stoeckli, *Electrochem. Commun.*, 16 (2012).
4. S. Q. Zhao, T. M. Liu, D. W. Hou, W. Zeng, B. Miao, S. Hussain, X. H. Peng, M. S. Javed, *Appl. Surf. Sci.*, 356 (2015) 259.
5. J. P. Cao, S. He, Y. Wu, X. Y. Zhao, X. Y. Wei, T. Takarada, *Int. J. Electrochem. Sci.*,12 (2017) 2704.
6. X. Du, W. Zhao, Y. Wang, C. Y. Wang, M. M. Chen, T. Qi, C. Hua, M. G. Ma, *Bioresourc. Technol.*, 149 (2013) 31.
7. Z. Peng, D. S. Zhang, T. T. Yan, J. P. Zhang, L. Y. Shi, *Appl. Surf. Sci.*, 282 (2013) 965.
8. B. B. Chang, Y. L. Wang, K. M. Pei, S. M. Yang, X. P. Dong, *RSC Adv.* 4 (2014) 40546.
9. J. N. Sahu, J. Acharya, B. C. Meikap, *Bioresourc. Technol.*, 101 (2010) 1974.
10. J. M. V. Nabais, C. Laginhas, M. M. L. R. Carrott, P. J. M. Carrott, J. E. C. Amorós, A.V.N. Gisbert, *Appl. Surf. Sci.*, 265 (2013) 919.
11. B. Xu, F. Wu, R. J. Chen, G. P. Cao, S. Chen, Z. M. Zhou, Y. S. Yang, *Electrochem. Commun.*, 10 (2008) 795.
12. X. J. He, Y. J. Geng, J. S. Qiu, M. D. Zheng, S. Long, X. Y. Zhang, *Carbon*, 48 (2010) 1662.

13. X. Y. Zhao, S. S. Huang, J. P. Cao, S. C. Xi, X. Y. Wei, J. Kamamoto, T. Takarada, *J. Ana. Appl. Pyrol.*, 105 (2014) 116.
14. M. Uğurlu, A. Gürses, Ç. Doğar, *Color. Technol.*, 123 (2007) 106.
15. X. J. He, P. H. Ling, M. X. Yu, X. T. Wang, X. Y. Zhang, M. D. Zheng, *Electrochim. Acta*, 105 (2013) 635.
16. I. Okman, S. Karagöz, T. Tay, M. Erdem, *Appl. Surf. Sci.*, 293 (2014) 138.
17. X. X. Xiang, E. H. Liu, L. M. Li, Y. J. Yang, H. J. Shen, Z. Z. Huang, Y. Y. Tian, *J. Solid State Electrochem*., 15 (2010) 579.
18. K. F. Fu, Q. Y. Yue, B. Y. Gao, Y. Y. Sun, L. J. Zhu, *Chem. Eng. J.*, 228 (2013) 1074.
19. W. Z. Zhang, M. Z. Zhao, R. Y. Liu, X. F. Wang, H. B. Lin, *Colloid. Surface. A.*, 484 (2015) 518.
20. W. H. Li, Q. Y. Yue, B. Y. Gao, X. J. Wang, Y. F. Qi, Y. Q. Zhao, Y. J. Li, *Desalination*, 278 (2011) 179.
21. J. Rouquerol, P. Llewellyn, F. Rouquerol, *Stud. Surf. Sci. Catal.*, 160 (2007) 49.
22. S. Yorgun, N. Vural, H. Demiral, *Micropor. Mesopor. Mat.*, 122 (2009) 189.
23. L. -Y. Hsu, H. Teng, *Fuel Process. Technol.*, 64 (2000) 155.
24. C. Peng, X. B. Yan, R. T. Wang, J. W. Lang, Y. J. Ou, Q. J. Xue, *Electrochim. Acta*, 87 (2013) 401.
25. Z. Z. Chang, B. J. Yu, C. Y. Wang, *Electrochim. Acta*, 176 (2015) 1352.
26. Z. Z. Chang, B. J. Yu, C. Y. Wang, *J. Solid State Electrochem.*, 20 (2016) 1405.
27. M. J. Bleda-Martínez, J. A. Maciá-Agulló, D. Lozano-Castelló, E. Morallón, D. Cazorla-Amorós, A. Linares-Solano, *Carbon*, 43 (2005) 2677.
28. L. Jiang, J. W. Yan, L. X. Hao, R. Xue, G. Q. Sun, B. L. Yi, *Carbon*, 56 (2013) 146.
29. H. Jiang, Y. J. Hu, S. J. Guo, C. Y. Yan, P. L. See, C. Z. Li, *Acs Nano.*, 8 (2014) 6038.
30. J. I. Hayashi, A. Kazehaya, K. Muroyama, A. P. Watkinson, *Carbon*, 38 (2000) 1873.
31. T. E. Rufford, D. Hulicova-Jurcakova, K. Khosla, Z. H. Zhu, G. Q. Lu, *J. Power Sources*, 195 (2010) 912.
32. M. Wu, P. Li, Y. Li, J. Liu, Y. Wang, *RSC Adv.*, 5 (2015) 16575.
33. E. Raymundo-Piñero, K. Kierzek, J. Machnikowski, F. Béguin, *Carbon*, 44 (2006) 2498.
34. S.T. Senthilkumar, B. Senthilkumar, S. Balaji, C. Sanjeeviraja, R. K. Selvan, *Mater. Res. Bull.*, 46 (2011) 413.
35. A. Elmouwahidi, Z. Zapata-Benabithe, F. Carrasco-Marin, C. Moreno-Castilla, *Bioresourc. Technol.*, 111 (2012) 185.
36. X. Du, P. Guo, H. Song, X. Chen, *Electrochim. Acta*, 55 (2010) 4812.
37. Y. J. Kim, B. J. Bee, H. Suezaki, T. Chino, *Carbon*, 44 (2006) 1592.
38. J. Sheng, C. Ma, Y. Ma, H. X. Zhang, R. R. Wang, Z. Y. Xie, J. L. Shi, *Int. J. Hydrogen Energ.*, 41 (2016) 9383.
39. M. Biswal, A. Banerjee, M. Deo, S. Ogale, *Energ. Environ. Sci.*, 6 (2013) 1249.
40. Z. B. Lei, J. T. Zhang, X. S. Zhao, *J. Mater. Chem.*, 22 (2012) 153.
41. Y. J. Huai, X. B. Hu, Z. J. Lin, Z. H. Deng, J. S. Suo, *Mater. Chem. Phys.*, 113 (2009) 962.
42. Z. Wang, X. Zhang, J. H. Wang, L. D. Zou, Z. T. Liu, Z. P. Hao, *J. Colloid Interf. Sci.*, 396 (2013) 251.
43. H. Hatakeyama, T. Hatakeyama, Springer-Verlag (2010), Berlin/Heidelberg, Germany.
44. M. Sevilla, R. Mokaya, *Energ. Environ. Sci.*, 7 (2014) 1250.
45. L. Yang, Y. Huang, H. Q. Wang, Z. Y. Chen, *Chem. Phy. Lipids*, 119 (2002) 23.